

# Nonlinear elastic and electronic properties of $\text{Mo}_6\text{S}_3\text{I}_6$ nanowires

I. Vilfan<sup>1</sup> and D. Mihailovic<sup>1</sup>

<sup>1</sup>*J. Stefan Institute, Jamova 39, SI-1000 Ljubljana, Slovenia*

(Dated: August 16, 2018)

The properties of  $\text{Mo}_6\text{S}_3\text{I}_6$  nanowires were investigated with ab initio calculations based on the density-functional theory. The molecules build weakly coupled one-dimensional chains with three sulfur atoms in the bridging planes between the Mo octahedra, each dressed with six iodines. Upon uniaxial strain along the wires, each bridging plane shows two energy minima, one in the ground state with the calculated Young modulus  $Y = 82$  GPa, and one in the stretched state with  $Y = 94$  GPa. Both values are at least four times smaller than the experimental values and the origin of the discrepancy remains a puzzle. The ideal tensile strength is about 8.4 GPa, the chains break in the Mo-Mo bonds within the octahedra and not in the S bridges. The charge-carrier conductivity is strongly anisotropic and the  $\text{Mo}_6\text{S}_3\text{I}_6$  nanowires behave as quasi-one-dimensional conductors in the whole range of investigated strains. The conductivity is extremely sensitive to strain, making this material very suitable for strain gauges. Very clean nanowires with good contacts may be expected to behave as ballistic quantum wires over lengths of several  $\mu\text{m}$ . On the other hand, with high-impedance contacts they are good candidates for the observation of Luttinger liquid behaviour. The pronounced 1D nature of the  $\text{Mo}_6\text{S}_3\text{I}_6$  nanowires makes them a uniquely versatile and user-friendly system for the investigation of 1D physics.

PACS numbers: 61.46.-w, 62.25.+g, 73.22.-f, 71.15.Mb

## I. INTRODUCTION

Inorganic nanowires and nanotubes are rapidly gaining in importance as materials of great scientific and technological interest because they exhibit a substantially enhanced level of functionality which can open novel opportunities for devices and applications. The main advantage of inorganic nanowires over other related materials is the possibility of controlling the relevant physical properties by selective engineering of their geometry and/or composition. Molybdenum-based inorganic nanowires and nanotubes in particular are emerging as materials with very promising physical properties because they are easier to functionalize and to synthesize in clean, single stoichiometry form than other one-dimensional materials. The synthesis, some physical properties and applications of several molybdenum-based nanowires have already been reported.<sup>1,2,3,4,5</sup> Recently, significant research effort has been focused on nanowires composed of Mo, chalcogens (S) and halogens (I) in the form  $\text{Mo}_6\text{S}_{9-x}\text{I}_x$  ( $\text{MoSI}_x$ ).<sup>6,7</sup> which are best described as molybdenum chalcogenide-halide polymers. They have a backbone skeleton composed of  $\text{Mo}_6$  octahedra, each dressed with six anions (S or I), bound together into one-dimensional chains by three bridging anions (either S or I). A specific feature of these materials is the growth of identical chains in the form of bundles. The materials have strong anisotropy, large Young moduli along the wires, very small shear moduli, and controllable electronic properties. In contrast to related nanowires such as  $\text{Li}_2\text{Mo}_6\text{Se}_6$  which decompose rapidly in air, the  $\text{MoSI}_x$  nanowires are entirely air-stable. Yang et al.<sup>7</sup> have recently investigated the  $\text{Mo}_{12}\text{S}_9\text{I}_9$  nanowires theoretically and have pointed out the bistable nature of the sulfur bridges, which allow the wires to stretch in an accordion-like fashion at vir-

tually no energy cost. They also pointed that strain can have a significant effect on the electronic band structure, and, interestingly, the appearance of a net spin polarisation within the nanowires in the unstrained position.

In this paper we report on the theoretical investigations of extraordinary elastic and electronic properties of the most common reproducibly synthesized  $\text{MoSI}_x$  nanowire material, namely  $\text{Mo}_6\text{S}_3\text{I}_6$ . Meden et al.<sup>6</sup> reported the structure where, after purification, the X-ray diffraction experiments indicated an iodine occupancy of the bridging atoms and only a small degree ( $\sim 10\%$ ) of disorder in the anion occupancies (either S or I). More recently, Nicolosi et al.<sup>8</sup> reported on the electron microscopy of same isomer with the same skeletal structure but with the bridging planes occupied by the sulfur atoms and all the iodines attached to the Mo octahedra. As we will comment later, both isomers have almost the same energy therefore it is possible that both are synthesized at similar rates. The question arises, how to identify them, what are the similarities and what are the differences between the two isomers. We shall concentrate in this paper on the isomer with three S atoms in the bridging planes, Fig. 1. From the tribology experiments we know that the interaction between individual nanowires is weak,<sup>9</sup> therefore we focus our analysis on the longitudinal properties of individual nanowires, ordered in a hexagonal array according to the spacegroup  $R\bar{3}c$ . This space group assumes the inversion symmetry which makes all the sulfur bridges equivalent. As a consequence we can scan the whole range of strains. Using the density-functional theory (DFT) we investigate the effect of strain on the elastic and electronic properties of these nanowires.

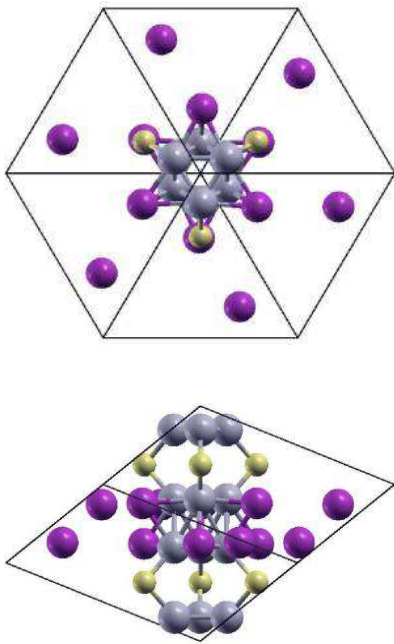


FIG. 1: (Color online) Top (upper panel) and side (bottom panel) view on the primitive cell of  $\text{Mo}_6\text{S}_3\text{I}_6$  nanowires ordered according to the spacegroup  $R\bar{3}c$ . Mo octahedra (grey) are dressed with 6 I atoms (violet - dark grey) and separated by 3 bridging S atoms (yellow - light grey). The X-ray scattering data and the DFT calculations of the  $R\bar{3}$  isomer indicate a  $\sim 6^\circ$  rotation of the chains around the hexagonal  $c$  axis and a certain degree of occupational (either S or I) disorder. The distant I atoms belong to the neighbouring chains.

## II. COMPUTATIONAL DETAILS

The structure and properties of Mo-S-I nanowires were analysed using the WIEN2k code.<sup>10</sup> The simulations were performed on a mixed basis set of augmented plane waves plus local orbitals (APW+lo)<sup>11</sup> for low orbital momenta ( $\ell \leq 2$ ) and linearized augmented plane waves (LAPW) for all the higher orbital momenta. The exchange and correlation potential was treated in the Perdew, Burke and Ernzerhof generalized-gradient approximation.<sup>12</sup> The muffin-tin radii were set to  $R_{\text{Mo}}^{\text{MT}} = 1.06 \text{ \AA}$  for Mo,  $R_{\text{S}}^{\text{MT}} = 1.27 \text{ \AA}$  for S, and  $R_{\text{I}}^{\text{MT}} = 1.38 \text{ \AA}$  for I, the kinetic energy cutoff was  $E_{\text{max}}^{\text{wf}} = 12.3 \text{ Ry}$  and the plane-wave expansion cutoff was  $E_{\text{max}}^{\text{pw}} = 196 \text{ Ry}$ .

First the hexagonal lattice constants  $a = b$ ,  $c$  and the atomic coordinates were optimized. In this stage the energy was calculated on a tetrahedral mesh with 44  $k$ -points in the irreducible part of the Brillouin zone. The same density of  $k$ -points was used for the analysis of elastic properties. Later, when calculating the electronic density of states, 189  $k$ -points were used. Since the interactions between neighbouring chains are weak, we kept the lattice constants  $a$  and  $b$  fixed, varied  $c$  and optimised the atomic coordinates when calculating the

properties of strained crystals. We thus obtain the elastic constants  $c_{11}$  which are close to the Young moduli  $Y$  because of weak interchain coupling.

## III. RESULTS

The DFT simulations of Mo-S-I arranged as shown in Fig. 1 give the equilibrium hexagonal lattice constants  $c = 11.56 \text{ \AA}$  and  $a = 16.54 \text{ \AA}$  which agree to within 3% with the experimental values  $c = 11.95 \text{ \AA}$  and  $a = 16.39 \text{ \AA}$  although we assumed a different spacegroup (the simulated group was  $R\bar{3}c$ , while the X-ray diffraction suggests  $P6_3$  or lower).<sup>6</sup> In this configuration the Mo-S-Mo angle across the bridging plane is  $90.8^\circ$ . Upon stretching the nanowires we find another energy minimum at  $c = 13.76 \text{ \AA}$  with the Mo-S-Mo angles  $145^\circ$ , Fig. 2(a). Yang et al.<sup>7</sup> ascribed the two equilibrium configurations to different s-p hybridizations of sulfur. However, inspection of the atomically resolved electron density of states, discussed later, shows very little s-p hybridization on sulfur. On the other hand, in the second energy minimum, the separation between the S atoms in the same bridging plane,  $d_{S-S} = 3.79 \text{ \AA}$ , is close to twice the van der Waals radius ( $r_{vdW} = 1.85 \text{ \AA}$ ) or to the separation between S in neighbouring layers in layered  $\text{MoS}_2$ ,  $d_{vdW} = 3.49 \text{ \AA}$ . Therefore we suggest the possibility that the van der Waals interaction between S on the same bridging plane stabilizes the second energy minimum.

The deeper minimum (unstrained wire) is subject to a potential barrier  $\Delta E = 0.47 \text{ eV}$  and the higher one by  $\Delta E = 0.26 \text{ eV}$ , both per formula unit. These barriers are too high to be thermally excited, the only way to move from one to the other minimum, is by applying an external stress.

### A. Elastic properties

Like other  $\text{MoSI}_x$  nanowires, also the  $\text{Mo}_6\text{S}_3\text{I}_6$  nanowires have large interchain separations with weak, van der Waals coupling between the chains. As a consequence, the nanowires are very anisotropic in their properties, including elasticity. They have large elastic constants in the direction of the wires,  $c_{11}$ , and small shear and Young moduli perpendicular to the wires. Here we shall concentrate on the most interesting elastic constant,  $c_{11} \approx Y$ .

We investigated the deformation of the  $\text{Mo}_6\text{S}_3\text{I}_6$  chains upon longitudinal tensile stress by keeping the lateral lattice constant  $a$  constant, to see how do the chains stretch and where are the weakest points in the chains. The corresponding calculated stress-strain diagram is shown in Fig. 2(b). Initially, most of the strain is connected to the deformation of the Mo-S-Mo bond angles across the bridging plane like in an accordion while the Mo-S distances and the structure of the Mo octahedra remain almost constant, (see Fig. 3). In this region the Young

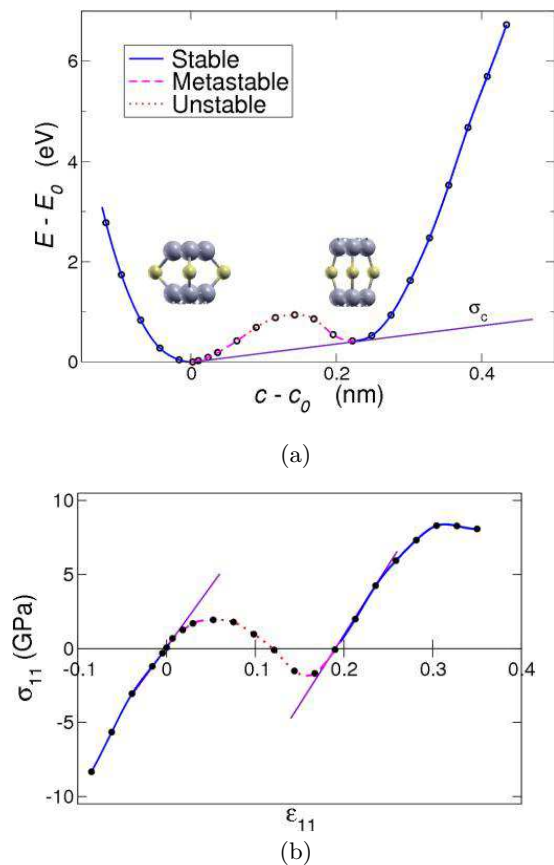


FIG. 2: (Color online) (a) Strain dependence of the binding energy per primitive cell (two  $\text{Mo}_6\text{S}_3\text{I}_6$  molecules). The two minima correspond to short and long Mo-S-Mo bridge configurations, respectively. In the unstable region the wire has short and long Mo-S-Mo bridges simultaneously. The inserts show the Mo-S-Mo bridges in the two energy minima. The straight line indicates the critical stress, i.e., the equilibrium transition between the two minima. (b) Stress-strain graph of  $\text{Mo}_6\text{S}_3\text{I}_6$  nanowires. The slopes of straight lines indicate the elastic constants of the two stable configurations. The maximum at  $\epsilon_{11} = 0.315$  is the ideal tensile strength of  $\text{Mo}_6\text{S}_3\text{I}_6$  nanowires with all the Mo-S-Mo bridges in the long configuration.

modulus is  $c_{11} = 82$  GPa. Very soon the value of the critical stress,  $\sigma_c = 0.39$  GPa is reached, (see Fig. 2(a)), when it becomes energetically more favourable for the Mo-S-Mo bonds to jump into their stretched configurations. However, the potential barrier between the two configurations prevents such transitions, the system remains in a metastable state (dashed line in Fig. 2) until the unstable region is reached when all the Mo-S-Mo bonds suddenly jump at constant stress to the stretched state. On contraction, upon reducing the stress, the Mo-S-Mo bonds remain in the stretched state down into the metastable region until they eventually jump into the slightly compressed state in the unstretched state. The  $\text{Mo}_6\text{S}_3\text{I}_6$  nanowires thus show a hysteresis in the stress-strain graph, caused by the potential barrier between the two energy minima which originate in the nature of the

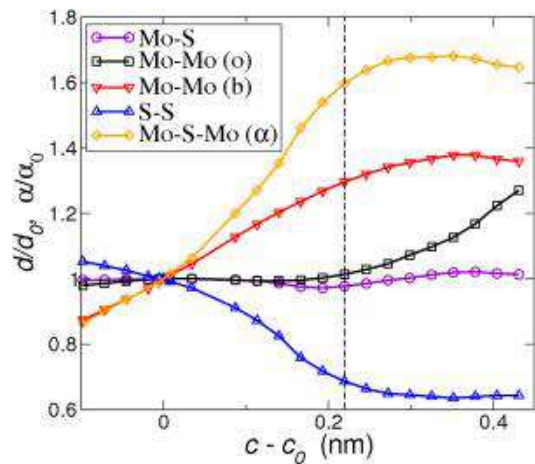


FIG. 3: (Color online) Variation of interatomic distances  $d$  and Mo-S-Mo angle  $\alpha$  upon stretching of  $\text{Mo}_6\text{S}_3\text{I}_6$  nanowires. Vertical dashed line shows the position of the second energy minimum. Mo-Mo (o) and (b) denote the Mo-Mo distances in the octahedron and across the bridge, respectively. The weakest segments where the wires break are the Mo octahedra.

Mo-S-Mo bonds across the bridging planes.

Of course, the Mo-S-Mo angles cannot open beyond  $180^\circ$ , and this is the reason for an increase in  $\sigma_{11}$  at large strains and for a higher elastic constant,  $c_{11} = 94$  GPa, than in the first energy minimum. The non-linear regime at higher  $\epsilon_{11}$  is the consequence of anharmonic forces and is not related to plastic deformation which is absent in our DFT calculations. Of course, the chains eventually break at the maximal stress. This defines the ideal tensile strength,  $\sigma_{\max} \approx 8.4$  GPa. Inspection of Fig. 3 tells us that the weakest links, where the chains break, are – surprisingly – the Mo octahedra and not the Mo-S-Mo bridges. This is also the reason why all  $\text{MoSI}_x$  nanowires have similar tensile strengths.

In the experiments the wires were subject to an initial stress which most probably brings all the Mo-S-Mo bridges into their stretched configurations. Only after this initial treatment the elastic constants were measured. Therefore one must compare the experimental elastic constant with that of stretched Mo-S-Mo bridge configurations. However, it remains a mystery, why the experimental longitudinal Young moduli exceed the elastic constants  $c_{11}$  reported in this paper by a factor of 4 or more.<sup>13</sup> The above values of  $c_{11}$  were calculated on a hexagonal array of molecular chain with all chains carrying equal load. For comparison, the Young modulus of a hexagonal array of single-wall carbon nanotubes (SWCNT) with the lattice spacing 1.7 nm is  $\sim 600$  GPa which is about 6 times the calculated value of  $c_{11}$ .<sup>14</sup>

The accordion effect is present also in other *one-dimensional* carbon chains like polyethylene or polyacetylene. What is unique to  $\text{Mo}_6\text{S}_4\text{I}_6$  is the double energy minimum. An additional sulfur in the centre of the bridging planes in  $\text{Mo}_6\text{S}_4\text{I}_6$  significantly increases the

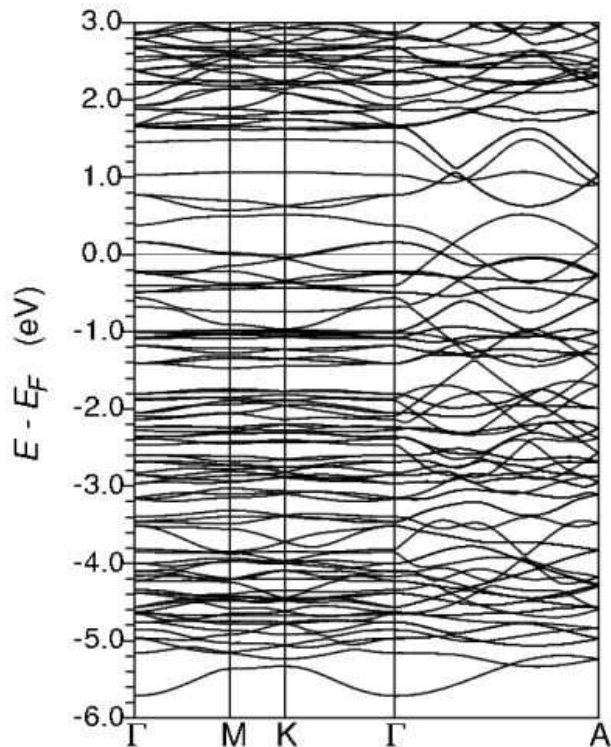


FIG. 4: Bandstructure of the conduction (valence) band along the special lines of the hexagonal Brillouin zone. Three sub-bands (one of them doubly degenerate) cross the Fermi energy and contribute to the charge carrier transport.

elastic constant ( $c_{11} = 114$  GPa), because it hinders the “accordion effect” of the Mo-S-Mo bonds. In case of  $\text{Mo}_6\text{S}_4\text{I}_6$  there is also no sign of a second energy minimum in strained nanowires. Finally we notice that the calculated elastic constant  $c_{11}$  of  $\text{Mo}_6\text{S}_3\text{I}_6$  is more than 3 times smaller than  $c_{11}$  of  $\text{Mo}_6\text{S}_6$  or  $\text{K}_2\text{Mo}_6\text{S}_6$  where the flexible Mo-S-Mo bridges are absent.<sup>15</sup>

### B. Electronic properties

The electron bandstructure of the conduction or valence band, Fig. 4, shows several interpenetrating sub-bands, three of them crossing the Fermi energy. Because of the anisotropy in the crystal structure the dispersion in the lateral directions is very small, we can classify  $\text{Mo}_6\text{S}_3\text{I}_6$  as a quasi-one-dimensional conductor. The conduction band consists of hybridized Mo-4*d*, S-3*p* and I-5*p* orbitals. The character of the sub-bands is most clearly seen in the electron density of states (DOS), Fig. 5. Close to  $E_F$  (region A in Fig. 5), the hybridization of the Mo-4*d* and S-3*p* states is the origin of good conduction along the Mo-S-I chains. This is not surprising since a conduction electron on its way along the chain must pass the sulfur bridges (S-3*p* states). This is also seen in the real-space charge-density plot in Fig. 6(a) where the charge density in the energy interval A is seen to run continu-

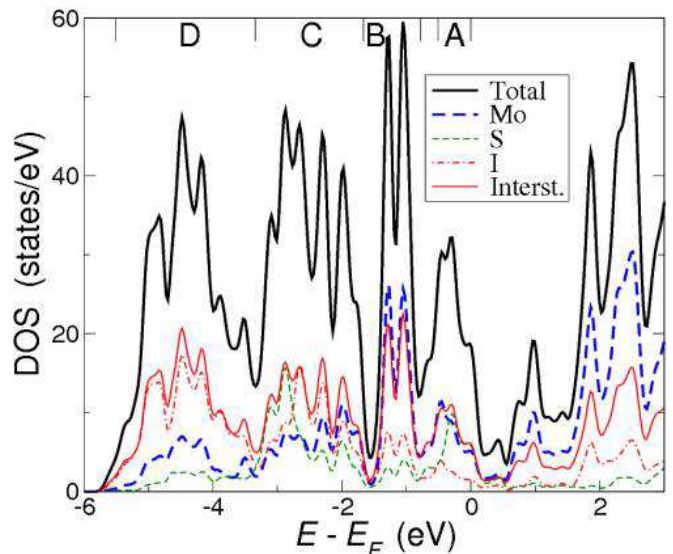


FIG. 5: (Color online) Density of states in the conduction (valence) band. For Mo, S and I the partial charges in the muffin-tin spheres are plotted, the rest are in the interstitial region. The main contributions to the conduction band are from Mo-4*d*, S-3*p* and I-5*p* orbitals. The letters at the top denote the energy ranges, discussed in the text.

ously throughout the chain. A cross-cut through the Mo (0001) plane, Fig. 6(b), reveals a combination of metallic bonds (with a uniform distribution of electrons within the Mo octahedron) and covalent bonds between neighbouring Mo atoms (a covalent bond is directional between the atoms). The I atoms, which are close to this plane, are only very weakly bound to the Mo octahedron in this energy window. Lower in energy, i.e., in energy window B, a strong Mo-4*d* double peak, also responsible for the Mo-Mo bonding, dominates the DOS.

Towards the bottom of the conduction band (energy interval D) the DOS is dominated by the states belonging to the dressing atoms (I-*p* in our case and S-*p* in case of  $\text{Mo}_6\text{S}_6$ <sup>15</sup>) and to polar covalent bonding between Mo and I.

The regions C and D of the conduction-valence band are mainly responsible for the Mo-S and Mo-I bonding. We identify these two bonds as polar covalent because of partial ionization of I and S. In fact, the charges of the muffin-tin spheres are as follows: Each Mo gives away 3.5 electrons, S 0.9 electrons and I 2 electrons, all these electrons fill the interstitial region. For comparison, Mo in metallic state gives away (into the conduction band) only two electrons. These charges are also in accordance with electronegativity. For a Mo-S bond the difference in electronegativity is 0.42 on the Pauling scale whereas for a Mo-I bond it is 0.50, I is slightly more negatively charged than S.

Comparison with the DOS of  $\text{Mo}_6\text{S}_6$  chains which have no S bridges,<sup>15</sup> shows similar occupations of Mo-4*d* states in both cases but a much weaker occupation of the S-3*p* states in case of  $\text{Mo}_6\text{S}_6$  close to  $E_F$ .



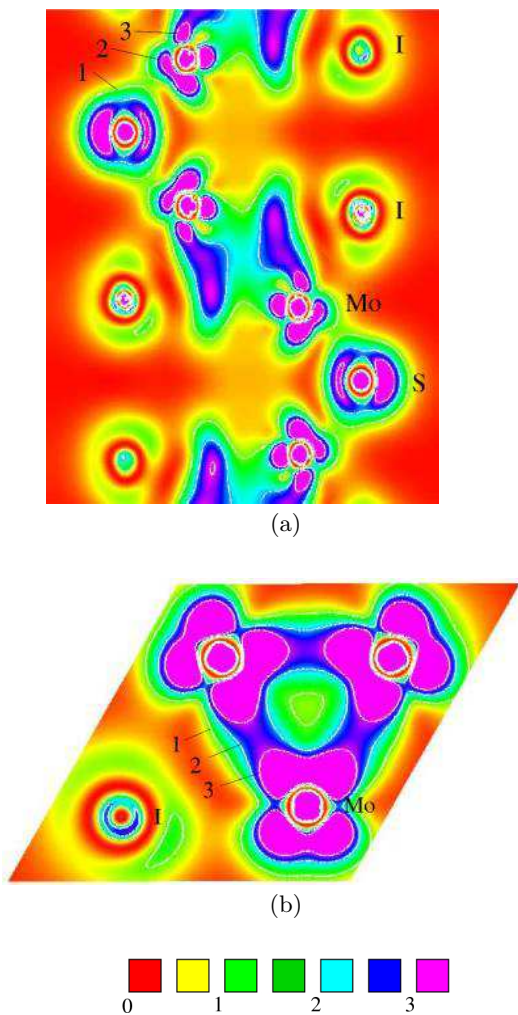


FIG. 6: (Color online) Valence charge density in the energy window A on the (1100) plane through the centre of a  $\text{Mo}_6\text{S}_3\text{I}_6$  nanowire (a) and on the (0001) plane through Mo atoms (b). The isolines and the color coding are in units of  $0.0167$  electrons/ $\text{\AA}^3$ . Clearly seen are the charge concentration on Mo octahedra and through the bridging sulfur atoms.

The bands below the conduction band are localized to the respective atoms and have well-defined characters with very little hybridization. In the whole DOS we see very little s-p hybridization in the sulfur orbitals from which we conclude that the s-p hybridization cannot be responsible for the stabilization of the second energy minimum at  $c = 13.7$   $\text{\AA}$  in  $\text{Mo}_6\text{S}_3\text{I}_6$ .

From Fig. 4 the estimated Fermi velocities are in the range between  $0.7$  and  $1.3 \times 10^6$  m/s. With a scattering lifetime  $\tau \sim 0.7 \times 10^{-14}$  s ( $\Gamma = 0.1$  eV) this leads to a mean free path along the wires of the order 5 to 9 nm, enough to justify a delocalized description of the charge carriers.

Comparison with the bandstructure of the  $\text{Mo}_6\text{S}_3\text{I}_6$  isomer with iodines in the bridging planes (spacegroup R3)<sup>6</sup> shows that the bandstructure is very sensitive to the anion occupancies, in particular to the occupancy

of the bridging atomic positions. Although the present R3c structure has virtually no calculated energy gap, the spacegroup R3 isomer has a  $\sim 0.6$  eV bandgap above  $E_F$ . According to our DFT calculations both structures have very similar formation energies, therefore we expect that both are synthesized simultaneously in comparable quantities. For the same reason we cannot exclude the presence of other  $\text{Mo}_6\text{S}_3\text{I}_6$  nanochains with more disorder in the anion occupancies. The bandstructure, the corresponding optical spectra and the longitudinal conductivity can be an effective criterion to distinguish between different isomers.

To gain insight on the conductivity behaviour we calculate the dielectric tensor  $\epsilon(\omega)$  in the random-phase approximation and in the limit  $q \rightarrow 0$ .<sup>17</sup> The static metallic conductivity is associated with the Drude peak which comes from transitions between states close to  $E_F$ . From the Drude peak damped with  $\Gamma = 0.1$  eV we find the longitudinal conductivity  $\sigma_{||} \sim 5 \times 10^3$  S/cm. This is a factor  $\sim 4$  lower than  $\sigma_{||}$  of  $\text{Mo}_6\text{S}_6$  nanowires, which we attribute to the weaker conduction of S bridges. The lateral conductivity is one order of magnitude smaller as well. This leads to a very short carrier mean free path in the lateral directions. Clearly the band picture breaks down in the lateral directions and the charge-carrier transport is via hopping between neighbouring chains. Of course, in real systems with finite-length chains the charge carriers must hop also between neighbouring chains and this can also hinder the charge carrier transport along the chains. In the calculation,  $\Gamma = 0.1$  eV was taken arbitrarily – for very clean nanowires,  $\Gamma$  could be substantially less and the conductivity correspondingly higher. With  $\Gamma = 0.1$  the longitudinal conductivity of  $\text{Mo}_6\text{S}_3\text{I}_6$  is about two order of magnitudes smaller than  $\sigma$  reported for SWCNT at 300 K which are considered to be one of the best one-dimensional conductors.<sup>16</sup>

### C. Electronic properties of stretched nanowires

The bandstructure of  $\text{MoSI}_x$  nanowires and consequently also the Fermi surfaces and electrical conductivity are extremely sensitive to strain along the hexagonal  $c$  axis. In Fig. 7 we show the bandstructure along the [001] symmetry direction for four different strains. Although it is difficult to follow a particular sub-band through the whole range of strains, we observe that in general the bandwidth of the sub-bands that cross  $E_F$  and which are responsible for the charge-carrier transport first increases with strain up to the second energy minimum ( $c = 13.7$   $\text{\AA}$ ) and then decreases. Not surprisingly, the bandwidth is related to the Mo-S distance, Fig. 3, which reaches its minimum around  $c = 13.7$   $\text{\AA}$ . Beyond  $c = 13.7$   $\text{\AA}$  the Mo-S distance increases and the sub-band width decreases, as expected. Similar behaviour is expected for the longitudinal DC conductivity. Above 15.2  $\text{\AA}$   $\sigma$  drops rapidly because the chains start to break apart. Assuming the same  $\Gamma$  in the lateral direction we find that the

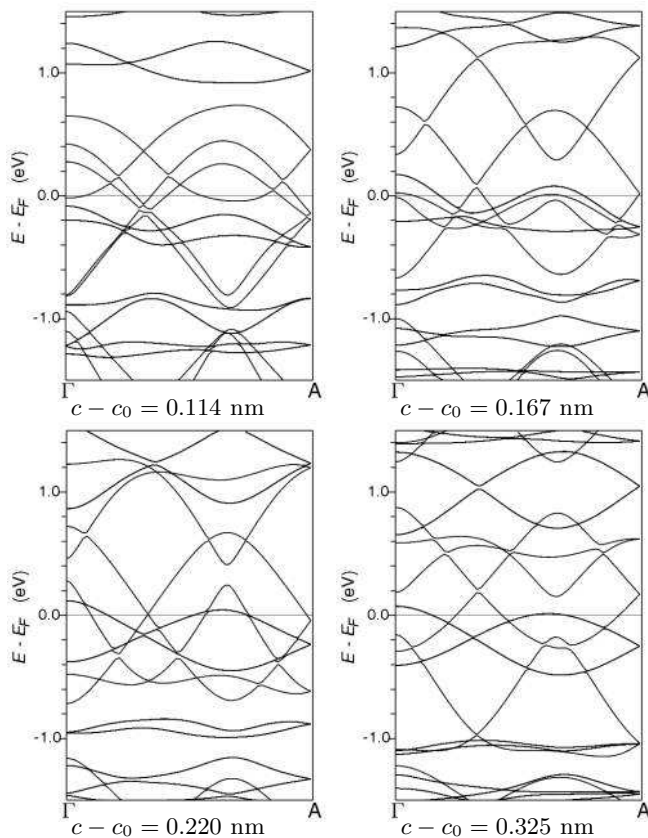


FIG. 7: Bandstructures of  $\text{Mo}_6\text{S}_3\text{I}_6$  nanowires subjected to longitudinal strain. Several sub-bands cross the Fermi energy and the width of these sub-bands is maximal close to the second energy minimum at  $c - c_0 = 0.220$  nm.

anisotropy in the static conductivity is large, typically of the order 100 for stretched nanowires. The Fermi surfaces of  $\text{Mo}_6\text{S}_3\text{I}_6$  in the second energy minimum ( $c = 13.76$  Å, Fig. 8) show typical features for a quasi-one-dimensional material, almost planar Fermi surfaces with very little curvature. The number of Fermi surfaces and the Fermi velocities are very sensitive to longitudinal strain, and so is the conductivity.

The  $\text{Mo}_6\text{S}_3\text{I}_6$  nanowires thus behave as quasi-one-dimensional metals in the whole range of strains. This is different to the  $\text{Mo}_{12}\text{S}_9\text{I}_9$  nanowires where a transition from metallic to narrow-gap semiconductor has been reported.<sup>7</sup>

The lateral conductivity is dominated by hopping to neighbour chains through the bridging sulfur atoms, see Fig.6. Upon longitudinal strain, the sulfur atoms move towards the centre of the wires whereas the interchain separation, dominated by the non-conducting I atoms, remains almost constant. As a consequence, the lateral conductivity drops rapidly with tensile strain.

The variation of the conductivity with strain is described with the strain gauge factor,  $G = \Delta\rho/(\rho\Delta\epsilon)$  where  $\rho = 1/\sigma$ . For the longitudinal conductivity we find  $G$  of the order -10 which is somewhere in between the

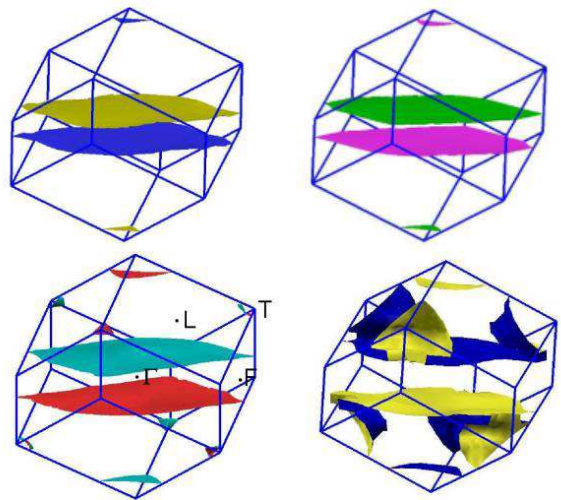


FIG. 8: Fermi surfaces and the Brillouin zone of the rhombohedral unit cell of stretched nanowires ( $c = 13.76$  Å).

typical values for semiconductors and for metals. However, the unusual feature of  $\text{MoSI}_x$  nanowires, and great potential advantage in applications is their extreme flexibility (large  $\Delta\epsilon$ ) arising from the accordion effect in the Mo-S-Mo bridges. Values of  $\Delta\sigma/\sigma \sim 1$  can be reached in the elastic regime which is an order of magnitude better than  $\Delta\sigma/\sigma$  in classical metallic strain gauges.

#### IV. DISCUSSION AND CONCLUSION

The  $\text{Mo}_6\text{S}_3\text{I}_6$  nanowires investigated in this paper have some similarities to the skeletally equivalent  $\text{Mo}_{12}\text{S}_9\text{I}_9$ , but also some important differences. Both nanowires have three sulfur atoms in the bridging planes between the Mo octahedra and each bridging plane shows two energy minima upon uniaxial strain, one in the ground state (unstretched wire) and one corresponding to the stretched wire. The potential barrier between the two minima is high and prevents thermally excited transitions between the two minima, it is responsible for hysteresis in the stress-strain behaviour of  $\text{Mo}_6\text{S}_3\text{I}_6$ . This interpretation is slightly different from Yang et al.<sup>7</sup> where the initial atomic configurations were subjected to random distortions, which of course mimic the entropy which helps to overcome the potential barriers in the metastable region.

Although the Mo-S-Mo bonds in  $\text{Mo}_6\text{S}_3\text{I}_6$  nanowires are very deformable, the Young modulus of the unstrained energy minimum is only slightly smaller than  $Y$  of the second minimum with strained Mo-S-Mo bonds. The lack of these very deformable Mo-S-Mo bridges in  $\text{Mo}_6\text{S}_6$  is also the reason why the latter chains have a higher Young modulus. Surprisingly, the chains break in the metallic-covalent bonds between Mo in octahedra and not, as one would expect, in the polar covalent Mo-S bonds across the S bridges. This is the reason why all Mo nanowires, dressed with I or S anions and with

or without bridging atoms, have similar calculated tensile strengths. However, the much larger experimental Young's moduli reported by Kis et al.<sup>13</sup> remain a puzzle at present. The Mo<sub>6</sub>S<sub>3</sub>I<sub>6</sub> nanowires behave as quasi-one-dimensional conductors in the whole range of investigated strains. The conductivity involves the Mo octahedra and the bridging atoms and is extremely sensitive to strain, making this material very suitable for strain gauges.

The fact that the experimentally reported shear modulus appears to be an order of magnitude smaller than in SWCNTs suggests that 1D effects will be even more pronounced than in SWCNT ropes, and the low-energy spectrum as  $E \rightarrow E_F$  is expected to be modified as a result. Very clean MoSI<sub>x</sub> nanowires with good contacts may be expected to behave as ballistic quantum wires over lengths of several  $\mu\text{m}$ . On the other hand, with high-impedance contacts MoSI<sub>x</sub> nanowires may be thought of excellent candidates for the observation of Luttinger liq-

uid behaviour<sup>18,19</sup>. Of course, one-dimensional metallic systems such as Mo<sub>6</sub>S<sub>3</sub>I<sub>6</sub> are subject to strong localisation effects. Defects on a molecular wire can effectively stop and localise electrons, whereupon hopping between molecular chains becomes relevant. The pronounced 1D nature of the nanowires makes them a uniquely versatile and user-friendly system for the investigation of 1D physics.

### Acknowledgments

We would like to acknowledge interesting discussions with A. Meden. This work was supported by the Slovenian Research Agency under the contract P1-0044. The crystal structures were visualized by Xcrysden.<sup>20</sup>

- 
- <sup>1</sup> M. Potel, R. Chevrel, M. Sergent, J.C. Armici, M. Decroux, and O. Fischer, *J. Solid State Chem.* **35**, 286 (1980).
- <sup>2</sup> J.M. Tarascon, F.J. DiSalvo and J.V. Warszczak, *Solid State Commun.* **52**, 227 (1984).  
J.M. Tarascon, G.W. Hull and F.J. DiSalvo, *Mat. Res. Bull.*, **19**, 915 (1984); J.M. Tarascon, *J. Electrochem. Soc.* **132**, 2089 (1985).
- <sup>3</sup> R. Brusetti, P. Monceau, M. Potel, P. Gougeon and M. Sergent, *Solid State Comm.* **66**, 181 (1988).
- <sup>4</sup> L. Venkataraman and C.M. Lieber, *Phys. Rev. Lett.* **83**, 5334 (1999).
- <sup>5</sup> F.J. Ribeiro, D.J. Roundy and M.L. Cohen, *Phys. Rev. B* **65**, 153401 (2002).
- <sup>6</sup> A. Meden, A. Kodre, J. Padeznik Gomilsek, I. Arcon, I. Vilfan, D. Vrbanic, A. Mrzel and D. Mihailovic, *Nanotechnology* **16**, 1578 (2005).
- <sup>7</sup> T. Yang, S. Okano, S. Berber, and D. Tománek, *Phys. Rev. Lett.* **96**, 125502 (2006).
- <sup>8</sup> V. Nicolosi, P.D. Nellist, S. Sanvito, E.C. Cosgriff, S. Krishnamurthy, W.J. Blau, M. L.H. Green, J. Sloan, D. Vengust, D. Dvorsek, D. Mihailovic, G. Compagnini, V. Stojan, J.D. Carey, and J.N. Coleman, to be published.
- <sup>9</sup> L. Joly Potuz, F. Dassenoy, J.M. Martin, D. Vrbanic, A. Mrzel, D. Mihailovic and W. Vogel, *Tribol. Lett.* **18**, 385 (2005).
- <sup>10</sup> P. Blaha, K. Schwarz, G.K.H. Madsen, D. Kvasnicka, and J. Luitz, WIEN2k, a full potential LAPW package (K. Schwarz, TU Vienna, 2001).
- <sup>11</sup> E. Sjöstedt, L. Nordström, and D.J. Singh, *Solid State Comm.* **114**, 15 (2000).
- <sup>12</sup> J.P. Perdew, K. Burke, and M. Ernzerhof, *Phys. Rev. Lett.* **77**, 3865 (1996).
- <sup>13</sup> A. Kis, G. Csanyi, D. Vrbanic, A. Mrzel, D. Mihailovic et al, to be published.
- <sup>14</sup> M.-F. Yu, B.S. Files, S. Arepalli, and R.S. Ruoff, *Phys. Rev. Lett.* **84**, 5552 (2000).
- <sup>15</sup> I. Vilfan, *Eur. Phys. J. B* **51**, 277 (2006).
- <sup>16</sup> A. Thess, R. Lee, P. Nikolaev, H. Dai, P. Petit, J. Robert, C. Xu, Y.H. Lee, S.G. Kim, A.G. Rinzler, D.T. Colbert, G.E. Scuseria, D. Tománek, J.E. Fisher, and R.E. Smalley, *Science* **273**, 483 (1996).
- <sup>17</sup> J. O. Sofo and C. Ambrosch-Draxl, *Comp. Phys. Commun.* **175**, 1 (2006).
- <sup>18</sup> K.A. Matveev and L.I. Glazman, *Phys. Rev. Lett.* **70**, 990 (1993).
- <sup>19</sup> L. Venkataraman, Yeon Suk Hong and P. Kim, *Phys. Rev. Lett.* **96**, 076601 (2006)
- <sup>20</sup> A. Kokalj: *J. Mol. Graphics Modelling*, **17**, 176 (1999). Code available from <http://www.xcrysden.org/>.